Nuclear Materials and Energy 37 (2023) 101509

Contents lists available at ScienceDirect

Nuclear Materials and Energy

journal homepage: www.elsevier.com/locate/nme

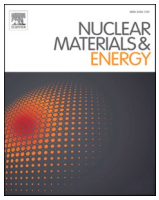

# The effect of nanocrystalline microstructure on deuterium transport in displacement damaged tungsten

S. Markelj [a,*], T. Schwarz-Selinger [b], M. Kelemen [a], E. Punzón-Quijorna [a], J. Zavašnik [a], A. Šestan [a], D. Dellasega [c,d], G. Alberti [c], M. Passoni [c,d]

[a] Jožef Stefan Institute, Ljubljana, Slovenia
[b] Max-Planck-Institut für Plasmaphysik, Garching, Germany
[c] Dipartimento di Energia, Politecnico di Milano, Milano, Italy
[d] Istituto per la Scienza e Tecnologia dei Plasmi, CNR, Milano, Italy

ARTICLE INFO

*Keywords:*
Grain boundaries
Deuterium
Tungsten
Transport
Displacement damage

ABSTRACT

The influence of grain boundaries (GBs) on the deuterium (D) transport and the creation of defects in nanocrystalline tungsten (W) films deposited on a W substrate was studied. Samples with three different grain sizes were produced for this purpose: a sample with a film having nanometer-size grains, a sample with hundred nanometer-grained film and a sample with micrometer-grained film. Samples were irradiated by 20 MeV W ions at 300 K to create displacement damage and exposed to 300 eV D ions at 450 K to populate the created and any pre-existing defects. The D transport and retention was assessed by measuring D depth profiles after certain exposure times by nuclear reaction analysis (NRA) using a $^3$He ion beam. From the final D concentration in the damaged area we could determine the concentration of defects that trap hydrogen, showing that the sample with the smallest grain size had the highest D concentration and it decreases with the increase of the grain size. Therefore, in nanocrystalline tungsten irradiated at 300 K, GBs do not improve radiation resistance, which would lead to fewer defects. For the first time, we show experimentally, that D transport is faster inside the nanometer-grained sample as compared to the micrometer-grained sample, meaning that D atoms have enhanced bulk diffusion along GBs. Accidentally, the film thickness was so thin that the W irradiation reached the interface between the W film and substrate, where NRA showed enhanced retention of oxygen. At that depth, two times higher D concentration was observed compared to D concentration in the damaged area in the middle of the film indicating on defect stabilization due to the presence of oxygen.

## 1. Introduction

In a future fusion reactor 14 MeV neutron irradiation will create displacement damage in tungsten (W) that is planned to be used as plasma-facing material. This will influence material properties, such as material ductility and strength. There is a discussion in the literature on how grain boundaries (GBs) can improve or impact displacement damage and hydrogen isotope transport. There are opposite opinions on what GBs can do. Some experiments show enhanced radiation tolerance in W by annihilation of defects at the GBs [1,2]. However, some experiments show an increased number of vacancies in nanostructured materials as compared to monocrystalline W [3,4]. In [4] the authors show that the number of vacancies is only reduced after annealing the samples to 573 K. Namely, due to the high vacancy mobility energy of 1.85 eV in W [5], only high temperature activates the vacancy motion to annihilate at the GBs. Fuel (deuterium and tritium) retention in future fusion devices is an important topic due to the safety and tritium self-sufficiency. When one discusses the interaction of hydrogen isotopes with GBs, density functional theory (DFT) calculations showed that GBs can be trapping sites for hydrogen isotopes [6,7]. Moreover, it was shown by theory and experiment that there is enhanced and fast diffusion of H atoms along certain grain boundaries with a diffusion barrier lower than in the bulk [6–9].

Our main interest in this subject is how GBs can affect hydrogen isotope transport and retention. The effect of microstructure on the transport was studied previously by our group, first in samples with the smallest grain size of 1–2 μm [10] and recently we extended the study down to nanometer grain size [11]. To create displacement damage, we

* Corresponding author.
*E-mail address:* sabina.markelj@ijs.si (S. Markelj).

https://doi.org/10.1016/j.nme.2023.101509
Received 7 August 2023; Accepted 8 September 2023
Available online 9 September 2023

used 20 MeV W ions which are a good proxy for neutron irradiation [12,13]. Deuterium (D) retention and transport were studied in [10,11] by exposing the samples to 0.3 eV deuterium atoms at 600 K. Regarding deuterium total retention no significant difference was observed between W single crystal, recrystallized polycrystalline W with 10–50 μm grain size and polycrystalline W with micrometer grain size [10]. All samples showed similar final D concentrations in the damage zone. Additionally, by decreasing the grain size to nanometer size [11] we observed a 20 % higher D concentration when comparing the nanometer-grained sample and micrometer-grained sample. Regarding the D transport, we have observed faster D uptake when decreasing the grain size, obtaining three times faster saturation of damaged layer with D in nanometer-grained samples compared to micrometer-grained sample [11]. With further increase of the grain size from micrometer to single crystal [10] the difference in D uptake time became smaller. In our first publication [10] we have explained this difference by increased uptake of D atoms at the surface due to larger grain boundary density at the surface. However, there is still a question of whether and how much the bulk diffusion along GBs also adds to this enhanced diffusion.

Now we have extended the study by exposing the different nanometer-grained samples, produced in the same way as in [11] to 300 eV D ions. In this case, the 300 eV D ions are directly implanted into the bulk of W and D can directly proceed to diffuse as mobile atoms. Oppositely, in the case of the 0.3 eV D atom exposure, surface processes first take place, where D atoms are adsorbed and chemisorbed at the surface. To penetrate into the bulk they need to overcome a large surface barrier of the order of 2 eV[14]. Only once in the bulk, they can diffuse as mobile atoms and populate the irradiation-induced defects. In both cases, the D energy (0.3 eV and 300 eV) and fluxes (few $10^{18}$ D/m$^2$s) are so low that no additional defects are induced [15] but only the existing defects are decorated. In our case these are the intrinsic defects and defects induced by 20 MeV W irradiation.

## 2. Sample production and experiment

Three W films were deposited on flat polycrystalline W substrates with dimensions of 10x20 mm$^2$, by pulsed laser deposition (PLD) at the energy department of Politecnico di Milano [16]. A laser pulse with a fluence of 15 J/cm$^2$ hits a W target. Due to the laser-matter interaction W is ablated at high energy (100 eV/atom) and expands in the vacuum chamber (base pressure $10^{-3}$ Pa). The W species deposit on a W substrate placed 7 cm away in front of the target at room temperature (no intentional heating is applied). The W film grows with a deposition rate of about 15 nm/min. W films with 3 μm thickness were planned to be deposited. The deposited W film is very compact and exhibits the same density of bulk W (19 g/cm$^3$). The crystalline W phase is α-bcc with (1 1 0) preferential orientation [16]. Part of the samples were vacuum-annealed (base pressure $5 \times 10^{-5}$ Pa) at 1023 and 1223 K (rate of 20 °C/min for heating/cooling ramps), using an internal heater, for 2 h of dwell time in order to tailor the grain size in the 100s nm range. One sample was left as deposited which resulted in nanometer-size grains. In this way, samples with three different grain sizes were produced. It is important to note that grain coarsening occurs at approximately 800 K; hence, the grain size should not change during D ion exposures at 450 K.

Samples were irradiated by 20.3 MeV W ions to a fluence of $7.8 \times 10^{17}$ ions/m$^2$ at 300 K in the TOF beamline at Max-Planck-Institut für Plasmaphysik (IPP), Garching [17]. For the chosen energy of 20.3 MeV SRIM 2008.04 [18] predicts displacement damage down to a depth of 2.3 μm with a peak at 1.35 μm for bulk tungsten as depicted in Fig. 2. With the film thickness of 3 μm, the plan was to create damage only in the deposited film. Evaluating the 'vacancy.txt' output of the 'Quick Calculation of Damage Option' of SRIM 2008.04 with a displacement threshold energy $E_D$ of 90 eV this converts to a primary damage dose in the damage peak of 0.23 dpa. In order to have a reference of an undamaged sample only halves of the samples were irradiated by the W beam. The damage dose was chosen such that we are in defect saturation for hydrogen-free tungsten. Namely, preceding studies with bulk W material and the same damaging procedure showed that D retention saturates at a damage level of around 0.1 dpa [12]. This was confirmed recently also by parameter-free modelling [19]. As a consequence, a flat distribution of defects and a constant D concentration through the damaged zone down to about 2 μm is expected.

The damaged W samples were exposed to deuterium ions with an energy of 300 eV/D at a temperature of 450 K. According to SRIM [18] the average implantation depth/maximum range is about 5 nm. The deuterium ion beam was created by a commercial ion gun Gen-II from TECTRA [20]. Compared with the D atom exposure experiments [10,11] a lower exposure temperature of 450 K was chosen in the present study to populate not only the high energy traps (most probably vacancy clusters) but also the ones with lower de-trapping energies (single vacancies, above approximately 1.35 eV) as was shown in [20]. The average D ion flux was $j = 3.5 \times 10^{18}$ D/m$^2$s. The exposure conditions were chosen such that no additional defects are created [15] but only the existing defects are populated.

The D depth profiles were measured by $^3$He NRA after different D ion exposure times and at the end of the exposure. The D ion beam size is such that it covers the whole W sample. Samples were exposed until the damaged area was fully saturated, meaning that the D concentration was homogeneous over the damaged area. The maximum exposure time for 300 eV D ions was 40 h, corresponding to a D fluence of $1.4 \times 10^{23}$D/m$^2$. The D($^3$He,p)$^4$He nuclear reaction was used [21] to analyze the retained deuterium with six different $^3$He energies ranging from 700 keV to 4.3 MeV. The NRA detector was positioned at an angle of 160° with respect to the probing beam. $^3$He beam size was 2 mm in diameter. Absolute quantitative, local information on the D concentration down to 7.2 μm was obtained by deconvoluting a measured proton energy spectra simultaneously with the software NRADC [22] and SIMNRA 6.02 [23]. From the NRA spectra measured with the $^3$He beam we could also determine the oxygen concentration in the films by utilizing the differential cross section for the $^{16}$O($^3$He,p$_0$)$^{18}$F nuclear reaction [24]. For this purpose, we fitted spectra measured at energies of 2.5 MeV, 3.3 MeV and 4.3 MeV using the SIMNRA program [23]. The information depth for oxygen is about 3 μm by using a 4.2 MeV $^3$He beam.

The grain size analysis of the thin films was conducted after D ion exposures on the undamaged halves of the samples using a dual-beam focused ion beam / scanning electron microscope (FIB-SEM, Helios Nanolab 650i, FEI) operating at 15 kV.

The D desorption spectra from the samples were measured 6 months after the D ion exposures and NRA analysis using thermal desorption spectroscopy (TDS), keeping the samples in a desiccator in the meantime. The TDS measurement was performed in the TESS set-up at IPP [25,26] using a linear heating ramp of 3 K/min up to 1010 K and a > 30 min hold at the highest temperature. The desorbed gases were measured with a Pfeiffer/ Inficon DMM 422 quadrupole mass spectrometer (QMS). The following 15 mass channels were recorded: $m/z = 1, 2, 3, 4, 12, 14, 16, 17, 18, 19, 20, 28, 32, 40,$ and 44. For the quantitative analysis, the QMS signal for $D_2$ was calibrated after each temperature ramp with a leak bottle from Laco Technologies with a flow of $1.22 \times 10^{14}$ $D_2$/s and a stated accuracy of 4.6%. The calibration factor for HD was determined by flowing HD through an orifice of known size from a calibrated volume of known absolute pressure (measured with a capacitance manometer and spinning rotor gauge) into the mass spectroscopy vessel. Based on the pressure recording of a calibrated spinning rotor gauge the calibration factor for HD molecules per measured QMS count was 62% of the one derived for $D_2$. To determine the amount of D desorbed during the measurement, masses 3 amu/q and 4 amu/q, corresponding to HD and $D_2$ molecules, respectively, were summed up. There was also some signal increase at masses 19 amu/q and 20 amu/q, corresponding to HDO and $D_2O$. The water calibration method is explained in [27]. The D signal coming from the water was added to the total D desorbed signal. The dominat D-water contribution was from HDO which contributed 10-15 % to the major D signal coming from $D_2$. The sample temperature during the TDS measurement was monitored directly using a sheathed thermocouple in direct contact with the sample. Since samples were only half irradiated by W ions, samples were cut

beforehand and TDS was performed on damaged halves of the samples.

## 3. Microstructural investigation

The thickness and the grain size of the deposited W films were analysed by SEM on film cross sections made by FIB. SEM images of the surfaces and sample cross sections are shown in Fig. 1 for all samples. In Fig. 1a,b and c surface and film cross section are shown for the "as deposited" film, respectively. This sample will be throughout the paper referred to as a nanometer-grained (nG) sample. The grain size analysis of the nG film showed a mean grain size distribution of 30 ±13 nm. The second sample, referred in continuation as a hundred-nanometer-grained sample (HnG), was annealed at 1023 K for 2 h. According to SEM analysis of sample FIB cross-section, shown in Fig. 1e and f, this resulted in grains up to 240 nm in size, with a mean grain size of 70 ± 39 nm. The third sample, the micrometer-grained (mG) sample, was annealed at 1223 K for 2 h which resulted in μm grain size. The analysis of the sample cross-section, shown in Fig. 1h and i, gave a mean grain size of 1026 ± 402 nm. From SEM images the estimated film thickness is 2 μm (Fig. 1b, e, h), which is shallower than the expected 3 μm.

Oxygen concentration in the films was determined by fitting the oxygen peak observed in the NRA spectra at different $^{3}$He energies. Oxygen concentration down to about 1.5 μm is 1 at. % and it increases to 3 at. % from 1.5 μm to 2 μm and then it decreases back to 1 at. % deeper in. The measured oxygen concentration was similar in all samples: in the as-deposited (nG sample) and annealed samples (HnG and mG).

A more detailed analysis of the films using transmission electron analysis and X-ray diffraction analysis was performed on samples used for the D atom exposures [11], that were prepared in the same way as the samples for the present study.

## 4. Deuterium retention results

The D depth profiles measured on the samples exposed to 300 eV/D ions at 450 K are shown in Fig. 2. The D depth profiles were measured after different exposure times to follow the transport of D into the samples. The measurements times were determined upon the beam time availability. At the end of exposure, we also measured the D depth profiles on the undamaged halves of the samples, shown in Fig. 2 as gray lines. In Fig. 2a we show the measured D depth profiles for the nG sample. The penetration of D ions was very fast and already after 4 h of exposure D reached the end of the damaged zone. The sample was exposed in total for 26 hours. In this case, the undamaged half was analysed after 22 h. The final maximum D concentration down to a depth of 1.5 μm of the nanometer-grained sample is 1.55 ± 0.01 at.%. The D concentration in the undamaged half of the sample in depth is 0.71 ± 0.03 at.%. In the case of the sample with the hundred-nanometer grains, Fig. 2b, the transport into the bulk was slower, and we observe that after 36 h D populated all the traps in the damaged zone. For the hundred-nanometer-grained sample the final maximum D concentration down to 1.5 μm depth on the damaged half is 1.51 ± 0.04 at.% and, therefore, very close to the nG sample. On the undamaged half of the sample the measured D concentration in depth is 0.06 ± 0.02 at.% and hence one order of magnitude less than for the nG sample. This indicates that the density of open-volume defects that trap deuterium decreased by one order of magnitude due to the annealing at 1023 K, since this was the temperature applied to increase the grain size. The observed trend of reduced uptake with increased grain size continues for the sample with micrometer grain size, Fig. 2c. In that case after 22 h D penetrated through the damaged zone and populated the defects there. After the additional 18 h of exposure (total 40 h) the D concentration increased only slighly around 2 μm. For this sample the final maximum D concentration measured within the damaged zone is 1.15 ± 0.03 at.% and hence slightly smaller than for the other two grain-sized samples. The concentration of D in the depth of the undamaged half is 0.04 ± 0.02 at.%, which is 30 % less than for the HnG sample.

A comparison of the D depth profiles between the damaged (full lines) and undamaged (dashed lines) halves of the samples after stop of the D ion exposure, are shown in Fig. 3 for all different-grained samples. Again, the SRIM-calculated damage depth profile is plotted to show how deep the damage zone reaches. These are the same D depth profiles as shown in Fig. 2 measured at the end of the exposure. The D depth profiles obtained on the undamaged half are also shown as dashed lines. We observe that the highest D concentration (1.55 at.%) is obtained for the nG sample. A slightly lower D concentration (1.51 at.%) was obtained on the HnG sample and the lowest was obtained on the mG sample (1.15 at.%). The D concentration on the undamaged half is also the highest for the nG sample (0.7at.%). The HnG and

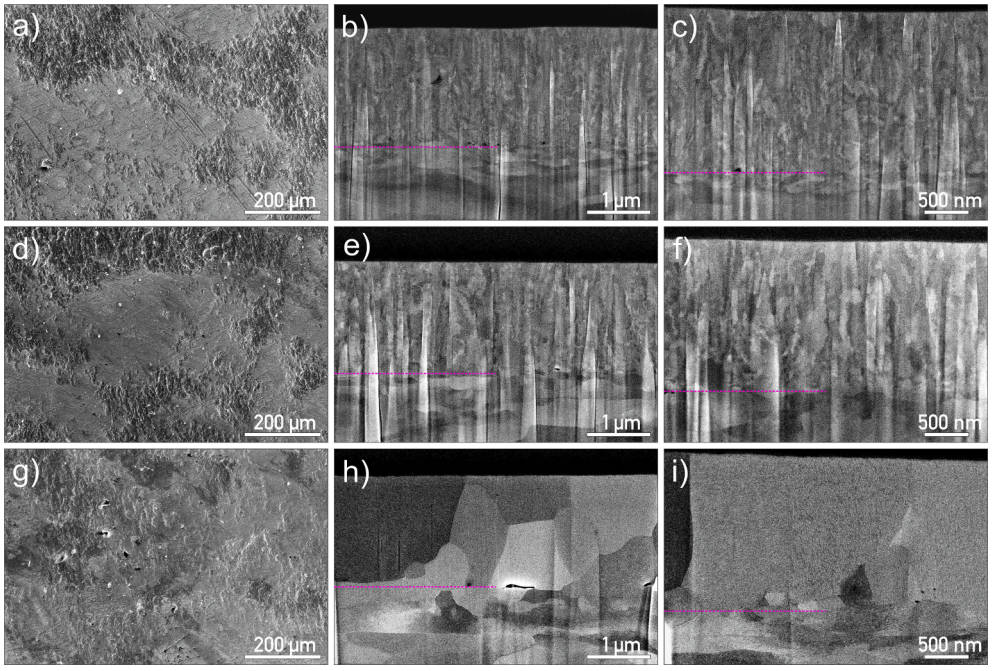


**Fig. 1.** SEM micrographs of the surfaces and cross-sections for the thin film samples with different grain sizes: a), b) and c) as-deposited film – "nanometer-grained" (nG) sample; d), e) and f) sample annealed at 1023 K for 2 h – "hundred-nanometer-grained" (HnG) sample; g), h) and i) sample annealed at 1223 K for 2 h – "micrometer-grained" (mG) sample with the corresponding marked deposited W layer (violet dash lines) on W substrate, topped by protective Pt deposit for FIB cutting.

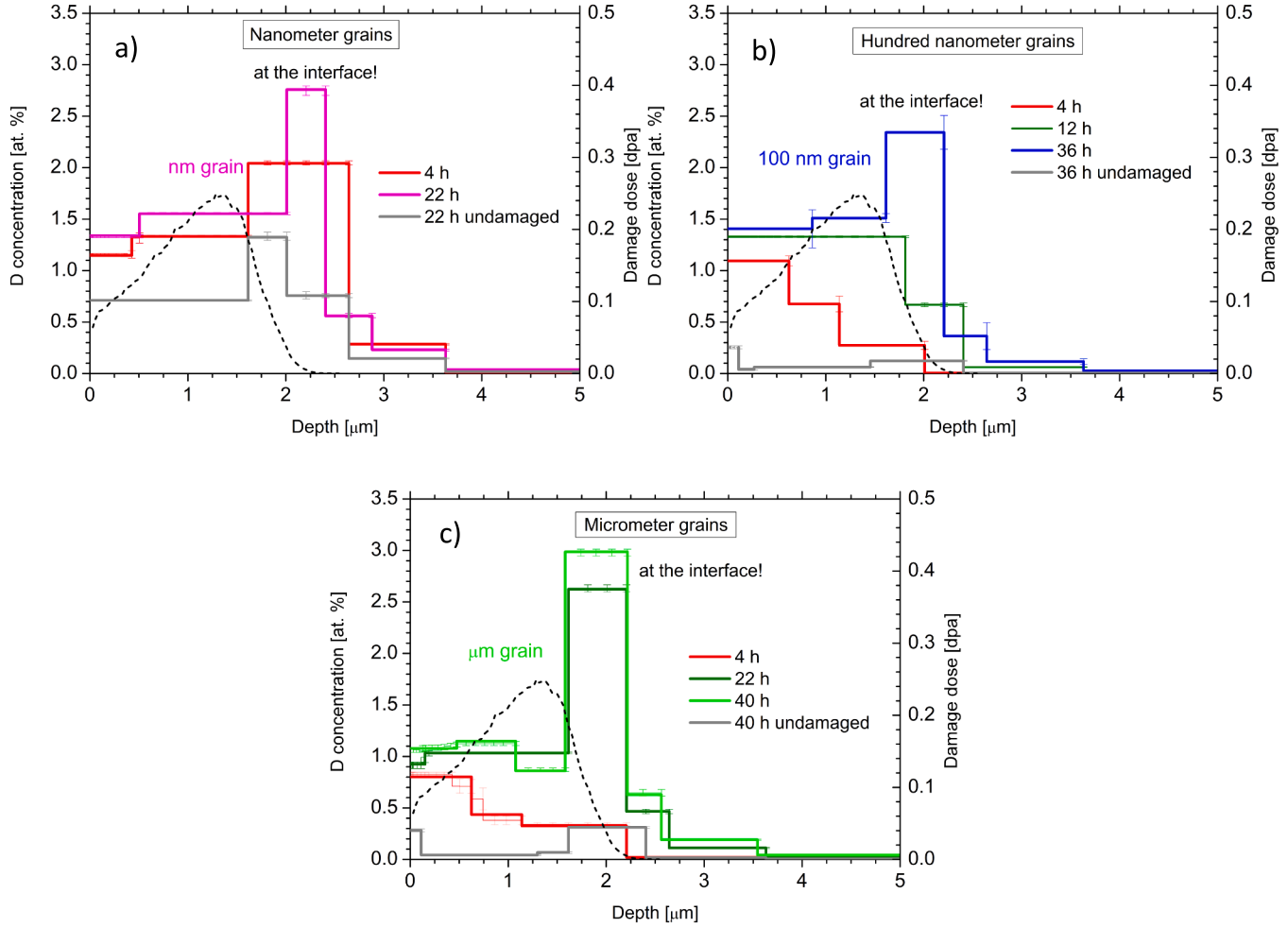


**Fig. 2.** D depth profiles as measured after certain time intervals and after stop of 300 eV D ion exposure at 450 K, a) for nanometer-grained (nG) sample, b) for hundred-nanometer-grained (HnG) sample and c) for the micrometer-grained (mG) sample. The D depth profiles obtained on the undamaged halves of the samples are also shown, grey lines. A SRIM calculated damage depth profile is also shown (dashed black line) with right Y scale.

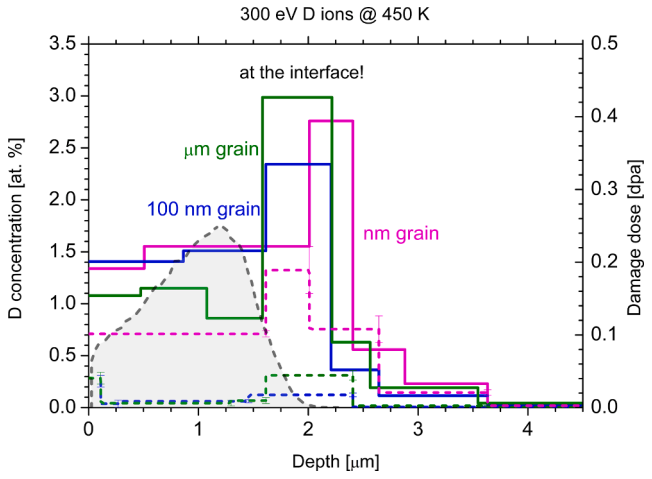


**Fig. 3.** D depth profiles measured at the end of the exposure to D ions at 450 K for all three types of samples. The D depth profiles obtained on the undamaged half of the sample are also shown as dashed lines. A SRIM calculated damage depth profile is shown as dashed black line with the right Y scale.

mG samples have very similar D concentration of 0.05 at.% down to about 1.6 μm in depth. One can also notice a large D concentration between 1.5 μm and 2.5 μm for all damaged samples, even larger than at 1.3 μm where, according to SRIM calculation, the maximum damage dose is induced. The D concentration there is almost two times higher (between 2.3 and 3 at. %) than in the mean damaged zone (from surface to 1.5 μm). Increase of D concentration between 1.5 μm and 2 μm is observed also for undamaged sample halves. D concentration beyond 3.5 μm drops by three orders of magnitude deeper inside where we have the polycrystalline W substrate. We believe that this increased D trapping has something to do with the interface between the film and the substrate, where increased oxygen concentration was detected by NRA. Namely, the layer thickness is only 2 μm and not 3 μm as initially planned. Due to the smaller layer thickness, W ion irradiation took place at the interface.

In Fig. 4, the D amounts from the surface down to 1.6 μm and within the whole analysed NRA depth, as a function of exposure time, are shown for the different-grained samples. We show both since the D amount beyond 1.6 μm is affected by the interface. The D total amount down to 1.6 μm for the nG sample reached 87 % of the maximum D amount ($152 \times 10^{15}$ D/cm$^2$) after 4 h whereas for the other two cases at this exposure time, the samples reached only approximately half of the maximum D amount (HnG – 52 % and mG – 49 %). The maximum D amounts down to 1.6 μm for HnG and mG samples are $148 \times 10^{15}$ D/cm$^2$ and $105 \times 10^{15}$ D/cm$^2$, respectively. The maximum was reached after about 12 h for the HnG sample. Unfortunately, for the mG sample the analysis was made only after 22 h and D reached its maximum probably somewhere between 4 and 22 h. In the case of the D amount within the whole analysed depth, the maximum was reached after about 35 h for HnG and mG samples but was reached already after 4 h for the nG

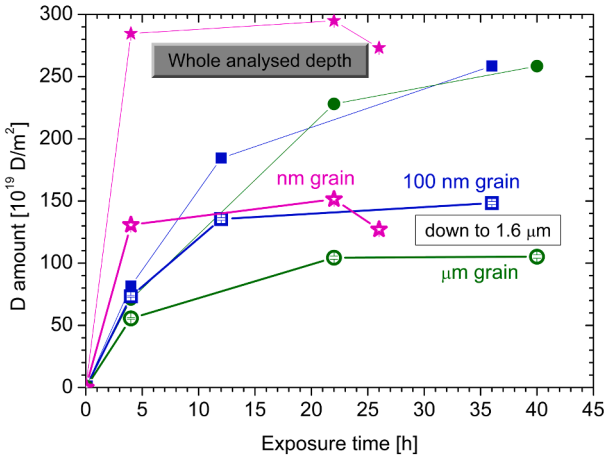


**Fig. 4.** D amounts as a function of exposure time for the different-grained samples exposed to 300 eV D ions at 450 K, as obtained from the D depth profiles shown in Fig. 2. The D amounts down to 1.6 μm (empty symbols) and D amounts within the whole analysed depth (full symbols) are shown.

sample. Interestingly, the D total amount within the NRA analyzed depth is the same for the HnG and mG samples, being (258.6 ± 1.4)× $10^{15}$ D/cm$^2$ and (258.5 ± 1.4)× $10^{15}$ D/cm$^2$, respectively, whereas for nG sample it is (273.1 ± 1.4) × $10^{15}$ D/cm$^2$.

The D desorption spectra as obtained by TDS are shown in Fig. 5 for the damaged halves of the studied samples. The desorption spectrum for nG is the highest and has three peaks: the highest first peak at 600 K, the second one at 750 K, and a small peak at 900 K with a tail. The spectrum for the HnG sample has the lowest D desorption compared to the other two samples and the first peak is somehow inclined with a maximum at 670 K and the small peak is at 820 K. The D desorption spectrum for mG sample attains the low-temperature peak at 620 K with similar intensity as the first peak of the nG sample and a shoulder at 820 K. For comparison, we also show the D desorption spectrum from a recrystallized polycrystalline tungsten (WR) also exposed to 300 eV D ions at 450 K [20]. The total D amount is not to be compared but only the shape, since the damage was performed by 10.8 MeV W ions, creating damage down to 1.3 μm. The peak shape in the nG sample is similar to the WR sample except that the first peak is higher and has a shoulder at 900 K continuing further with a tail. The HnG and mG samples do not have a peak at 750 K but only a shoulder at 820 K, meaning that there is fewer defects with a de-trapping energy of about 1.86 eV and more defects with de-trapping energy

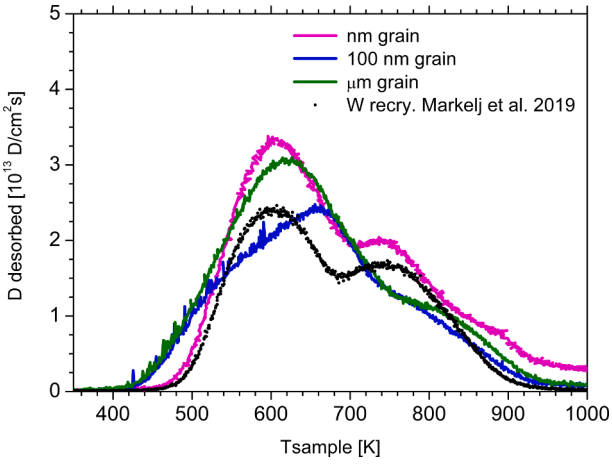


**Fig. 5.** D desorption spectra obtained on the damaged halves of the nanometer-grained, hundred-nanometer-grained, and micromete-grained samples. We show also the D desorption spectrum obtained on recrystallized polycrystalline W exposed to 300 eV D ions at 450 K, taken from [29]. The linear heating ramp was 3 K/min.

of 2.1 eV (see Fig. 4 in [28]). The total D desorption amounts as obtained by TDS are 154 × $10^{15}$ D/cm$^2$, 119 × $10^{15}$ D/cm$^2$and 140 × $10^{15}$ D/cm$^2$ for nG, HnG and mG samples, respectively. Comparing the TDS D total amounts, we obtain only 56 %, 46 % and 54 % of the NRA D total amounts for nG, HnG and mG samples, respectively. The fact that we detect only half of the D amount by TDS as compared to NRA indicates that D outgassing is larger for the studied films as compared to damaged and recrystalized polycrystalline W, where at most 6-9 % outgassing was observed after 1.5 years [13].

## 5. Discussion

Concerning the influence of GBs on the D transport there is a drastic change, obtaining about 3 times faster uptake, when comparing the nG sample with the other two samples. This clearly indicates that we have preferential D diffusion along the GBs which is the fastest for the sample that has the highest density of grain boundaries, confirming the theoretical calculations [3,6,8]. Also concerning the evolution of the depth profile, one can observe that in the case of the nG sample, D reached the end of the damaged region very quickly and with further exposure only the D concentration increased. In the case of HnG and mG samples there is a moving front of D penetrating into the bulk

From the obtained D desorption peaks for the studied samples when compared with the polycrystalline W exposed to D ions at 450 K [28,29] (having the same linear heating ramp of 3 K/min) we see that the desorption peaks are in the same temperature range. This means that the D de-trapping energies range from 1.35 to 2.05 eV, where the individual de-trapping energies were attributed to three different trap types, recognized in the literature as single vacancies and different sizes of vacancy clusters [28]. Considering the fact that the D concentration and D amount is not vastly different between the different grained sample and that D desorption peaks are similar, this means that GBs do not influence significantly D trapping at an exposure temperature of 450 K. This cleraly shows that D populates the formed vacancies and vacancy clusters inside the grains or at the GBs after it diffused along the GBs. DFT calculations [6] gave H migration energy $E_{dif}$ of 0.13 eV which is 0.07 eV lower than the migration barrier for H in the bulk [3,31,31]. Since the difference in migration energy is not very large, there is a probability (exp(-$E_{dif}$/$k_B$T)) that for 1 out of 7 jumps, D atom will jump back into the bulk. Considering the fact that by TDS we have obtained only about 50 % of the NRA total D amount, indicates that GBs offer also path for room temperature D de-trapping from the defects, during the storage time. This is not observed to such an extent in polycrystalline W [13].

In the introduction, when discussing the faster transport in nano-grained material in the D atom case [10,11], we gave two possible explanations for the faster D uptake with a higher density of GBs or smaller grain size. Namely, either the surface plays the major role where higher GB density on the surface increases D uptake from the surface into the bulk (surface effect), or there is a bulk effect, where a larger density of GBs increases diffusion along the grain boundaries in the bulk itself. In the case of D ion exposure with an energy of 300 eV/D, ions are directly implanted into the bulk. Therefore, the surface cannot play a big role. Hence, we can exclude here the influence of the surface and we can conclude that the observed faster uptake is due to faster D diffusion along the grain boundaries inside the nanocrystalline sample. We show a schematic picture comparing a polycrystalline W and a nano-grained W [32]. The faster diffusion along the GBs increases D uptake and population of defects in the grains. This is additionally confirmed by the observed effect of the different evolution of the D depth profiles in the nG sample compared to the mG sample, where D quickly reached the end of the damaged zone and then D concentration increased homogeneously. This was even more pronounced for the D atom exposures [11].

Regarding the effect of GB on defect creation we have observed that the D concentration in the damaged zone is the highest for the nG sample but the D concentration in the HnG sample is only slightly lower. The lowest D concentartion was obtained for the mG sample. This is

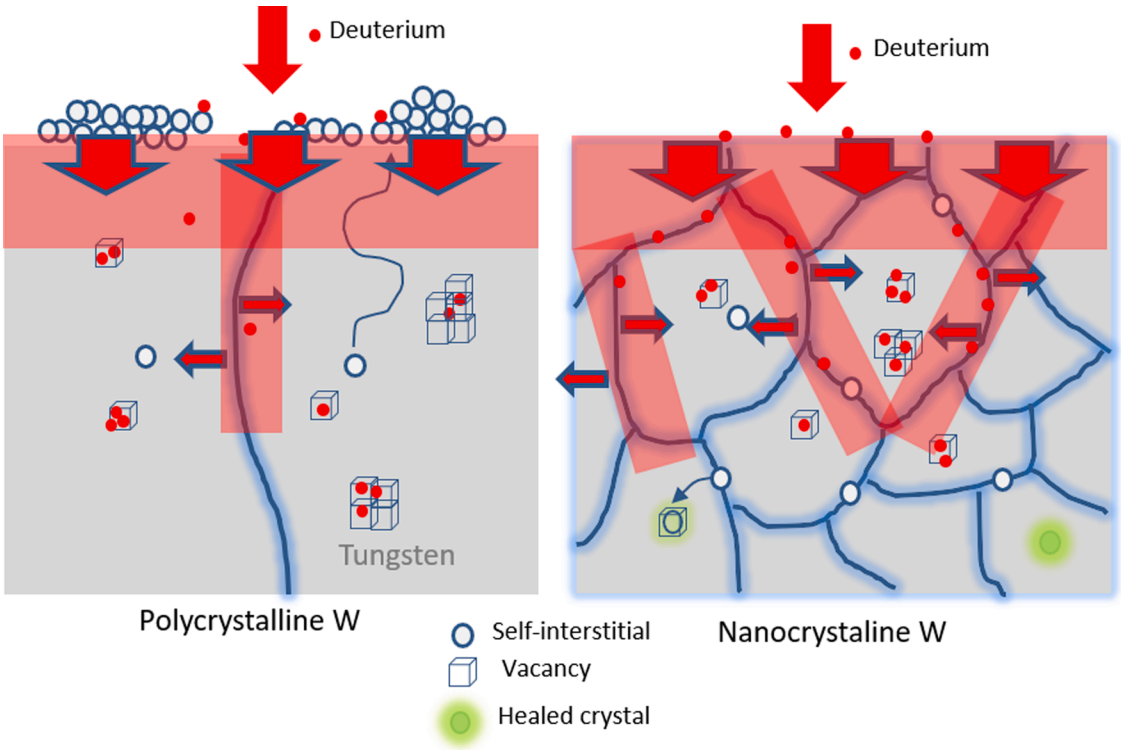


**Fig. 6.** Schematic figure of polycrystalline and nanocrystalline W sample and how the D diffusion proceeds in both cases together with the self-interstitial diffusion and D population of vacancies and vacancy cluster that were created within the grain due to W irradiation.

summarized in Fig. 7, where we show the maximum D concentrations as a function of grain size for irradiated and undamaged W samples. Comparing nG and mG samples, the difference in D concentration is 35 %. In the case of D atom exposure, we observed a 20 % difference [11]. The larger difference in D concentration for the 300 eV D ion case could be due to the lower exposure temperature for the D ion case. Therefore, one could conclude that no substantial defect annihilation at grain boundaries was observed for W irradiation at 300 K. However, the as-deposited layer of the nG sample showed a high D concentration indicating on a lot of defects due to the manufacturing process that are present in the sample before the W ion irradiation. A similar effect was observed in [33]. With the annealing procedure to tailor the grain size, the defects were substantially reduced in the undamaged samples. For comparison, we show D concentration for WR, data taken from [20]. Also, in other studies higher hydrogen retention was observed for nanograined samples as compared with samples with micrometer grains [3]. Therefore, GBs do influence Frenkel pair annihilation but in an opposite manner. According to [34–36] GBs affect self-interstitial (SIA) and vacancy annihilation in three different temperature regimes: i) At low temperatures where there is a high mobility of SIAs, SIAs can migrate and get trapped at GBs, which leads to higher vacancy density in nanostructured as compared to monocrystalline materials. ii) At intermediate temperatures, the SIAs retained at the GBs are emitted, migrate inside grains and annihilate with vacancies. iii) At high temperatures, vacancies become mobile and migrate, finding GBs at which they annihilate. In the case of W, there is a vastly different mobility energy between SIAs, being 0.13 eV [37,38], and vacancies, being 1.85 eV [5,37]. Therefore, for our W irradiation at a temperature of 300 K, SIAs can migrate and due to the large density of GBs in the nanocrystalline sample, they are annihilated at the GBs, whereas vacancies are immobile and stay where they were created. This results in a higher vacancy concentration in the vicinity of the grain boundaries within the diffusion length of SIAs and consequently results in a higher D concentration for samples with a larger density of GBs. In polycrystalline W SIAs have to travel a long way to reach either the surface or grain boundaries and there is therefore a higher chance that they annihilate with a vacancy on its way, leading to the lower amount of vacancies (schematically shown in Fig. 6). From the experiment, we can conclude that the difference is not drastic, of a few ten percent.

When comparing the maximum D concentration for the atom (0.3–0.35 at. %) [10,11] or ion exposed samples (1.1–1.5 at %), we obtain more than a factor of four higher D concentration for the D ion exposure. This is not because a different species was used but because different temperature was applied during D loading, 450 K for ions and 600 K for atoms. Namely, at lower exposure temperature one can populate defects that have lower trapping energies. The trend for D concentration is the same in both cases, the highest is for the nG sample and the other two follow [11]. Interestingly the difference in the D

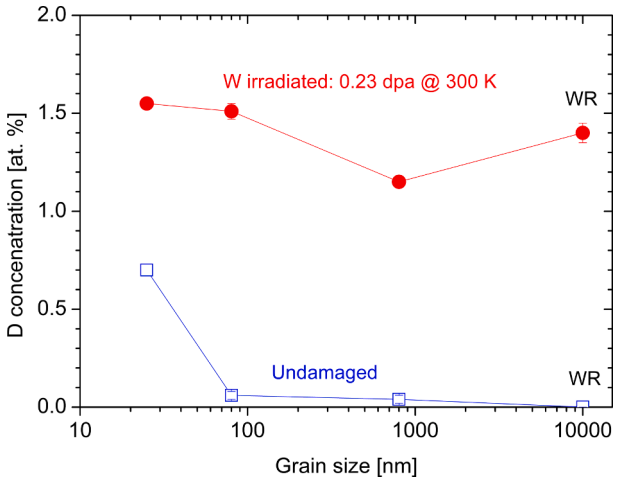


**Fig. 7.** Maximum D concentration obtained on the damaged (W irradiated) and undamaged halves of the samples as a function of grain size. The last point is shown for recrystallized polycrystalline W (WR) from [20].

uptake is also three times faster in the case of atoms in the nG sample compared to the HnG sample even though the temperature was higher in the atom case and the D concentration was lower. This clearly indicates that the transport is along the GBs and that the GB diffusion is not the rate-limiting process.

The last point to be discussed is the phenomenon observed at the interface. There is a clear increase in the D concentration at the interface, where D concentration is almost two times higher than the D concentration measured at the SRIM-calculated damage peak. The reason for this is not clear since if there are additional traps, then the increase should be similar to what was measured on the undamaged half. The difference between undamaged and damaged halves is the W ion irradiation, which in the damaged samples reached the interface, consequently increasing the concentration of defects by a factor of two. By NRA we have observed an increased oxygen amount at the interface as compare to the bulk. TEM analysis of the samples prepared for D atoms exposures [11] showed also crystalline tungsten oxide at the interface. Therefore, in both cases we have oxygen at the interface, however, for D atom exposure, such an increase in D concentration was not observed. The only difference is that here the film is thinner (2 μm) and the W irradiation took place also at the interface. One could speculate that oxygen presence at the interface stabilized the defects during the W irradiation, increasing the defect concentration that traps D, as was observed for deuterium [20,28] and predicted by DFT calculations [39]. If there would be only the effect of oxygen on the D retention then the D increase should be similar as is observed on the undamaged half, where the D concentration increased by about 0.5 at. % and not by 1.5 at. % as is the case for damaged halves.

## 6. Conclusions

We have studied D retention and transport in samples with different grain sizes. The study was performed with 300 eV/D ions at 450 K. We have shown that the D transport is the fastest in the sample with the smallest grain size. This clearly proves that GBs increase transport in the bulk and that there is preferential D diffusion along the GBs being the fastest for the sample with the highest GB density, confirming the theoretical calculations. Regarding the damage creation we have observed that the D concentration in the damaged zone is highest for the nG sample. D concentration on the HnG sample is slightly lower and for the micrometer-grained sample is the lowest. Therefore, when displacement damage takes place at 300 K, the fast diffusing SIAs get annihilated at GB leaving excess of vacancies in nanograined W, as compared to W with lower GB density. Finally, W irradiation of the interface leads to two fold increase of the D concentration as compared to the D concentration within the irradiated film, indicating on defect stabilization due to the presence of oxygen.

## CRediT authorship contribution statement

**S. Markelj:** Conceptualization, Formal analysis, Writing – original draft, Visualization, Investigation, Recources. **T. Schwarz-Selinger:** Formal analysis, Writing – review & editing, Investigation. **M. Kelemen:** Investigation. **E. Punzón-Quijorna:** Investigation. **J. Zavašnik:** Writing – review & editing, Investigation, Formal analysis. **A. Šestan:** Investigation, Formal analysis. **D. Dellasega:** Writing – review & editing, Investigation. **G. Alberti:** Investigation. **M. Passoni:** Writing – review & editing, Investigation, Resources.

## Declaration of Competing Interest

The authors declare that they have no known competing financial interests or personal relationships that could have appeared to influence the work reported in this paper.

## Data availability

Data will be made available on request.

## Acknowledgments

This work has been carried out within the framework of the EUROfusion Consortium, funded by the European Union via the Euratom Research and Training Programme (Grant Agreement No 101052200 — EUROfusion). Views and opinions expressed are however those of the author(s) only and do not necessarily reflect those of the European Union or the European Commission. Neither the European Union nor the European Commission can be held responsible for them. This work was supported by IAEA Coordinated Research Project F43025, entitled 'Hydrogen Permeation in Fusion-Relevant Materials'. The authors acknowledge the support from the Slovenian Research Agency, research core funding No. P2-0405.

## References

[1] O. El-Atwani, et al., In-situ TEM/heavy ion irradiation on ultrafine-and nanocrystalline-grained tungsten: effect of 3MeV Si, Cu and W ions, Mater Charact 99 (2015) 68–76.
[2] O. El-Atwani, et al., Loop and void damage during heavy ion irradiation on nanocrystalline and coarse grained tungsten: microstructure, effect of dpa rate, temperature, and grain size, Acta Materialia 149 (2018) 206–219.
[3] G. Valles, et al., Influence of grain boundaries on the radiation-induced defects and hydrogen in nanostructured and coarse-grained tungsten, Acta Mater. 122 (2017) 277–286.
[4] M. Panizo-Laiz, et al., Experimental and computational studies of the influence of grain boundaries and temperature on the radiation-induced damage and hydrogen behavior in tungsten, Nucl. Fusion 59 (2019), 086055.
[5] J. Heikinheimo, et al., Direct observation of mono-vacancy and self-interstitial recovery in tungsten, APL Mater. 7 (2019), 021103.
[6] H.-B. Zhou, et al., Investigating behaviours of hydrogen in a tungsten grain boundary by first principles: from dissolution and diffusion to a trapping mechanism, Nucl. Fusion 50 (2010), 025016.
[7] T. Oda, Thermodynamic model for grain boundary effects on hydrogen solubility, diffusivity and permeability in poly-crystalline tungsten, Fusion Eng. Des. 112 (2016) 102–116.
[8] U.V. Toussaint, S. Gori, Modeling hydrogen transport in large disordered systems, Phys. Scr. T159 (2014), 014058.
[9] P. Díaz-Rodríguez, et al., Direct observation of hydrogen permeation through grain boundaries in tungsten, Emergent Mater. 5 (2022) 1075–1087.
[10] M. Pečovnik, S. Markelj, A. Založnik, T. Schwarz-Selinger, Influence of grain size on deuterium transport and retention in self-damaged tungsten, J. Nucl. Mater. 513 (2019) 198.
[11] S. Markelj, et al., Influence of grain boundaries on deuterium retention and transport in ion-irradiated tungsten, submitted to Nucl. Mater. Energy.
[12] O.V. Ogorodnikova, V. Gann, Simulation of neutron-induced damage in tungsten by irradiation with energetic self-ions, J. Nucl. Mater. 460 (2015) 60.
[13] B. Wielunska, M. Mayer, T. Schwarz-Selinger, A.E. Sand, W. Jacob, Deuterium retention in tungsten irradiated by different ions, Nucl. Fusion 60 (2020), 096002.
[14] E.A. Hodille, A. Založnik, S. Markelj, T. Schwarz-Selinger, C.S. Becquart, R. Bisson, C. Grisolia, Simulations of atomic deuterium exposure in self-damaged tungsten, Nucl. Fusion 57 (2017) 056002.
[15] E.A. Hodille, N. Fernandez, Z.A. Piazza, M. Ajmalghan, Y. Ferro, Hydrogen supersaturated layers in H/D plasma-loaded tungsten: a global model based on thermodynamics, kinetics and density functional theory data, Phys. Rev. Mater. 2 (2018), 093802.
[16] D. Dellasega, G. Merlo, C. Conti, C.E. Bottani, M. Passoni, Nanostructured and amorphous-like tungsten films grown by pulsed laser deposition, J. Appl. Phys. 112 (2012), 084328.
[17] T. Schwarz-Selinger, Deuterium retention in mev self-implanted tungsten: influence of damaging dose rate, Nuclear Mater. Energy 12 (2017) 683–688.
[18] J. Ziegler, "www.srim.org.," [Online].
[19] D.R. Mason, et al., Parameter-free quantitative simulation of high-dose microstructure and hydrogen retention in ion-irradiated tungsten, Phys. Rev. Materials 5 (2021), 095403.
[20] S. Markelj, et al., Displacement damage stabilization by hydrogen presence under simultaneous W ion damage and D ion exposure, Nucl. Fusion 59 (2019), 086050.
[21] B. Wielunska, M. Mayer, T. Schwarz-Selinger, U. von Toussaint, J. Bauer, Cross section data for the D(3He, p)4He nuclear reaction from 0.25 to 6MeV, Nucl. Instr. and Meth. Phys. Res. B 371 (2016) 61.
[22] K. Schmid, U. von Toussaint, Nucl. Instr. and Meth. Phys. Res. B 281 (2012) 64.
[23] M. Meyer, SIMNRA User's Guide, Report IPP 9/113, Max-Planck-Instutut für Plasmaphysik 1997 Garching, Germany [Online]. Available:.
[24] M. Guitart Corominas, T. Schwarz-Selinger, Experimental determination of the 16O (3He, p0)18F differential cross section, Nucl. Instrum. Methods Phys. Res., Sect. B 450 (2019) 13–18.
[25] E. Salançon, T. Dürbeck, T. Schwarz-Selinger, F. Genoese, W. Jacob, J. Nucl. Mater. 376 (2008) 160.
[26] T. Schwarz-Selinger, J. Bauer, S. Elgeti, S. Markelj, Influence of the presence of deuterium on displacement damage in tungsten, Nucl. Mater. Energy 17 (2018) 228–234.

[27] K. Kremer, M. Brucker, W. Jacob, T. Schwarz-Selinger, Influence of thin surface oxide films on hydrogen isotope release from ion-irradiated tungsten, Nucl. Mater. Energy 30 (2022), 101137.
[28] M. Pečovnik, E.A. Hodille, T. Schwarz-Selinger, C. Grisolia, S. Markelj, New rate equation model to describe the stabilization of displacement damage by hydrogen atoms during ion irradiation in tungsten, Nucl. Fusion 60 (2020), 036024.
[29] S. Markelj, T. Schwarz_Selinger, A. Zaloznik, M. Kelemen, P. Vavpetic, P. Pelicon, E. Hodille, C. Grisolia, Deuterium retention in tungsten simultaneously damaged by high energy W ions and loaded by D atoms, Nucl. Mater. Energ. 12 (2017) 169–174.
[30] N. Fernandez, Y. Ferro, D. Kato, Hydrogen diffusion and vacancies formation in tungsten: density functional theory calculations and statistical models, Acta Mater. 94 (2015) 307–318.
[31] K. Heinola, T. Ahlgren, Diffusion of hydrogen in bcc tungsten studied with first principle calculations, J. Appl. Phys. 107 (2010), 113531.
[32] G. Ackland, Controlling Radiation Damage, Science 327 (2010) 1587–1588.
[33] O.V. Ogorodnikova, Effect of nanostructure on radiation tolerance and deuterium retention in tungsten, J. Appl. Phys. 122 (2017), 044902.
[34] I.J. Beyerlein, et al., Radiation damage tolerant nanomaterials, Mater. Today 16 (2013) 443–449.
[35] X.-M. Bai, B.P. Uberuaga, The influence of grain boundaries on radiation-induced point defect production in materials: a review of atomistic studies, JOM 65 (2013) 360–373.
[36] X.-M. Bai, A.F. Voter, R.G. Hoagland, M. Nastasi, B.P. Uberuaga, Efficient annealing of radiation damage near grain boundaries via interstitial emission, Science 327 (2010) 1631–1634.
[37] C.S. Becquart, C. Domain, U. Sarkar, A. DeBacker, M. Hou, Microstructural evolution of irradiated tungsten: Ab initio parameterisation of an OKMC model, J. Nucl. Mater. 403 (2010) 75–88.
[38] P.M. Derlet, D. Nguyen-Manh, S.L. Dudarev, Multiscale modeling of crowdion and vacancy defects in body-centered-cubic transition metals, Phys. Rev. B 76 (2007), 054107.
[39] X.-S. Kong, et al., The role of impurity oxygen in hydrogen bubble nucleation in tungsten, J. Nucl. Mater. 433 (2013) 357–363.